# Measurement of xenon plasma properties in an ion thruster using laser Thomson scattering

Yamamoto, Naoji
Department of Advanced Energy Engineering Science, Kyushu University

Tomita, Kentaro
Department of Applied Science for Electronics and Materials, Kyushu University

Sugita, K

Kurita, T

他

https://hdl.handle.net/2324/23217

# Measurement of xenon plasma properties in an ion thruster using laser Thomson scattering technique

N. Yamamoto, K. Tomita, K. Sugita, T. Kurita, H. Nakashima et al.

## Related Articles

Diagnosis of gas temperature, electron temperature, and electron density in helium atmospheric pressure plasma jet
Phys. Plasmas 19, 073513 (2012)

Numerical studies of third-harmonic generation in laser filament in air perturbed by plasma spot
Phys. Plasmas 19, 072305 (2012)

Molybdenum emission from impurity-induced m = 1 snake-modes on the Alcator C-Mod tokamak
Rev. Sci. Instrum. 83, 10E517 (2012)

2D full wave modeling for a synthetic Doppler backscattering diagnostic
Rev. Sci. Instrum. 83, 10E331 (2012)

Thomson scattering diagnostic for the measurement of ion species fraction
Rev. Sci. Instrum. 83, 10E323 (2012)
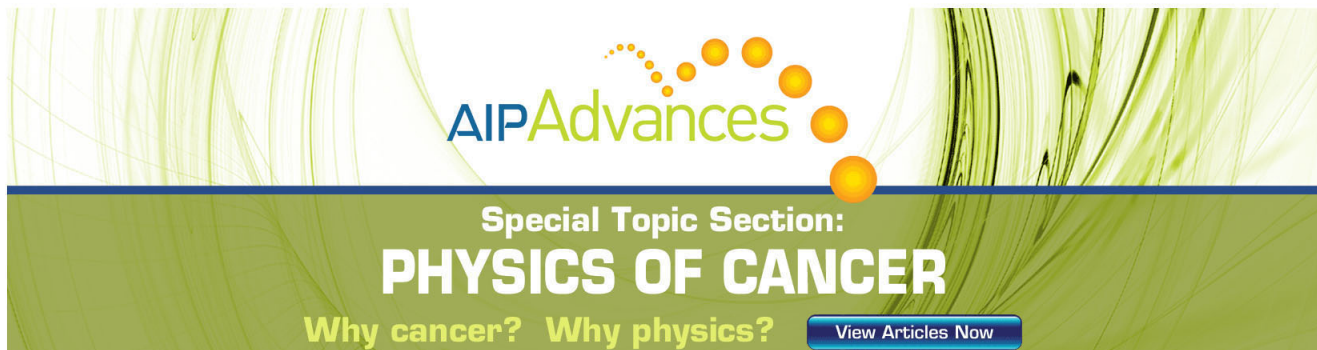
## Additional information on Rev. Sci. Instrum.

# Measurement of xenon plasma properties in an ion thruster using laser Thomson scattering technique

N. Yamamoto, K. Tomita, K. Sugita, T. Kurita, H. Nakashima, and K. Uchino
*Kyushu University, 6-1 Kasuga-kouen, Kasuga, Fukuoka 816-8580, Japan*

This paper reports on the development of a method for measuring xenon plasma properties using the laser Thomson scattering technique, for application to ion engine system design. The thresholds of photo-ionization of xenon plasma were investigated and the number density of metastable atoms, which are photo-ionized by a probe laser, was measured using laser absorption spectroscopy, for several conditions. The measured threshold energy of the probe laser using a plano-convex lens with a focal length of 200 mm was 150 mJ for a xenon mass flow rate of 20 $\mu$g/s and incident microwave power of 6 W; the probe laser energy was therefore set as 80 mJ. Electron number density was found to be $(6.2 \pm 0.4) \times 10^{17}$ m$^{-3}$ and electron temperature was found to be $2.2 \pm 0.4$ eV at a xenon mass flow rate of 20 $\mu$g/s and incident microwave power of 6 W. The threshold of the probe laser intensity against photo-ionization in a miniature xenon ion thruster is almost constant for various mass flow rates, since the ratio of population of the metastable atoms to the electron number density is little changed. © *2012 American Institute of Physics*. [http://dx.doi.org/10.1063/1.4737144]

## I. INTRODUCTION

An ion thruster is a rocket engine that works by pushing ions away from the spacecraft. Ions produced in the discharge chamber are propelled by the electric field generated by a pair of grids. Ion thrusters show high energy transfer efficiency, exceeding 70%, with good specific propellant consumption.[1] Therefore, ion thrusters have already been used extensively in space missions, such as Deep Space I,[2] HAYABUSA,[3,4] and others,[5] and will be used in the future missions.

The development of ion thrusters will depend to some extent on the ability to measure plasma properties in the vicinity of a screen grid (one of the ion extraction grids); electron number density and electron energy distribution function (EEDF) are of particular interest. Furthermore, this information will play an important role in the validation of numerical models for lifetime estimation.[6] There have been many studies of plasma properties inside the discharge chamber,[7] and these results have contributed to the development of ion thrusters. Using intrusive methods, however, it has been difficult to measure the plasma properties in the vicinity of the screen grids without disturbing the plasma. Non-intrusive methods are therefore required for these measurements. One such technique is Laser Thomson Scattering (LTS).[8] LTS is a laser-based optical method for a measurement of plasma properties, such as electron number density ($N_e$) and electron temperature ($T_e$). In the incoherent regime, the scattered spectrum reflects the Doppler motion of individual electrons, and the scattered intensity is proportional to $N_e$. This method was developed to measure plasma properties in high temperature plasma having $N_e > 10^{19}$ m$^{-3}$.[9] During the last two decades, its applicability has been extended to plasma with densities of less than $10^{16}$ m$^{-3}$, by a signal accumulation technique.[10] The signal accumulation technique is described in detail in Refs. 10 and 11. It permits application of LTS to the plasma in the discharge chamber of a miniature microwave ion thruster;

our previous study showed that the LTS technique is a useful tool for the measurement of plasma properties and can facilitate improvement of thrust performance.[12] The laser, however, induced some perturbation in the xenon plasma due to photo-ionization of excited xenon atoms;[13] metastable xenon atoms are ionized by the laser (wavelength 532 nm and photon energy 2.3 eV).

The aim of the present study was to measure the electron temperature/number density of xenon plasma in ion thrusters. In order to prevent photo-ionization, the threshold energy of photo-ionization effect was investigated. Then, the plasma properties were measured below the threshold using the LTS technique. The population of metastable xenon atoms $(6s[3/2]^0_2)$ was also measured by laser absorption spectroscopy (LAS).[14–16]

## II. EXPERIMENTAL SET-UP

### A. Ion thruster

The cross section of a 30 W class miniature microwave discharge ion thruster is shown in Fig. 1. The thrust performance of our ion thruster, that is, thrust and thrust efficiency, are 0.79 mN and 0.57, respectively, at a xenon mass flow rate ($\dot{m}$) = 18 $\mu$g/s, and total input power of 28 W (incident microwave power, $P_i$, of 8 W).[17,18] This performance is competitive with that of the thruster developed by Wirz, which has hitherto shown the best performance in this class of miniature thruster.[19] The inner diameter of the discharge chamber is 21 mm and the length is 12 mm. The overall size of the thruster is 50 mm × 50 mm × 30 mm. The ion source consists of an antenna and a magnetic circuit, which is made up of several samarium cobalt (Sm-Co) permanent magnets and iron yokes. The magnetic field strength inside the discharge chamber can be changed by changing the number of the permanent magnets. For this study, twelve magnets were used,
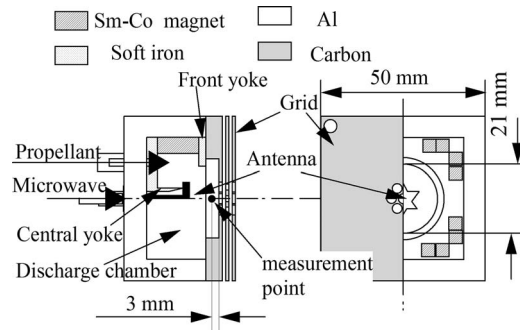
FIG. 1. Cross section of a 30 W class miniature microwave discharge ion thruster.



FIG. 2. Experimental setup for LTS measurements.

for easy ignition and good performance. The magnetic mirrors are located at the tip of a front yoke and the tip of a central yoke. Microwave power at 2.45 GHz is fed through a coaxial line and into the antenna. A DC block with a loss of 0.43 dB at 2.45 GHz was inserted to protect the microwave amplifier. A 1 mm thick, star shaped antenna was used, since it has showed good performance in previous studies.[18] The antenna is inscribed in a 9 mm diameter circle and is made of molybdenum. Flat square grids were used to extract the ion beam; the geometric parameters are shown in Table I. This geometry was designed using a numerical analysis code developed by Arakawa *et al.*[20] The grids are made of isotropic graphite, and ceramic insulators are used as isolators between the three grids. The gap between the grids is 0.5 mm and the ion beam diameter is 12 mm.

A 0.3 m diameter by 0.4 m long vacuum chamber was used in the experiments, with a turbo molecular pump with overall pumping speed of 150 l/s for air. The background pressure was maintained below $1.0 \times 10^{-2}$ Pa for most of the operating conditions. High-purity (99.9995%) xenon gas was used as the propellant. A thermal mass flow controller with a flow rate error of less than 5% for most conditions was used. The estimated pressure inside the discharge chamber was 0.3 Pa at $\dot{m} = 20$ $\mu$g/s, considering that the conductance of the thruster is $1.3 \times 10^{-3}$ m³/s and the background pressure was $4 \times 10^{-3}$ Pa. In this study, the ion beam was not extracted.

### B. Laser Thomson scattering measurement system

Figure 2 shows the experimental setup for LTS measurements on the miniature microwave discharge ion thruster. The scattering light inside the discharge chamber is collected

TABLE I. Grid parameters.

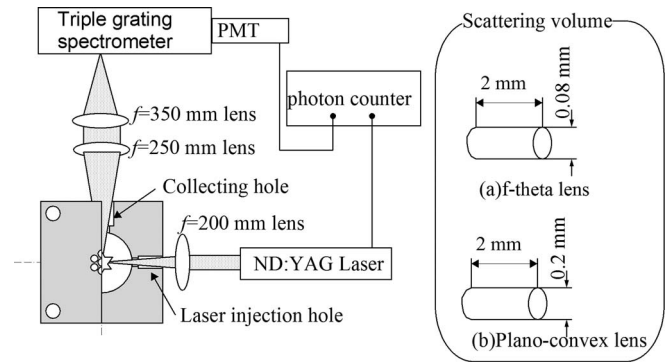| Parameter | Screen grid | Accel. grid | Decel. grid |
|---|---|---|---|
| Hole diameter, mm | 3.0 | 1.8 | 3.0 |
| Potential, V | 1200 | −200 | 0 |
| Thickness, mm | | 1.0 | |
| Hole pitch, mm | | 3.50 | |
| Material | | Isotropic graphite | |
| Grid gap, mm | | 0.5 | |
| Number of holes | | 7 | |

through a hole ($\phi = 3$ mm) and the laser beam passes through two small holes ($\phi = 2$ mm). The $\phi = 3$ mm hole is positioned at an angle of 90 degree to the laser pass.

The light source is the second harmonic beam of an Nd:YAG laser having a wavelength of 532 nm with a maximum energy of 200 mJ, a repetition rate of 10 Hz, a pulse width of 6 ns and a beam divergence of 0.6 mrad. The measurement point is 3 mm upstream of the screen grid on the thruster axis ($z$ axis). The laser beam is focused through a focusing lens (focal length, $f$, 200 mm). We use an $f$-theta lens and a plano-convex lens; the size of the focal spots with the $f$-theta lens and with the plano-convex lens were estimated by observing the Rayleigh scattering spatial profile from 40 kPa air gas, and found to be 80 $\mu$m and 165 $\mu$m in diameter, respectively. Scattered light from the plasma is focused onto the entrance slit of a Triple Grating Spectrometer (TGS) with two achromatic lenses of $f = 350$ mm and $f = 250$ mm. The slit width is 200 $\mu$m. The scattering volume is 0.165 × 0.165 × 2 mm³, as determined by the laser beam size, slit width and slit height, respectively. The solid angle of observation is about 0.025 sr. Strong stray light is generated from the surface of the components, due to the small size of discharge chamber, and the LTS signals are overwhelmed by it. In order to reduce stray light, the discharge chamber wall was made of carbon and the TGS was used. The scattered light is dispersed by passing through the TGS, and is detected by photo-multiplier tube (PMT). The TGS used in this experiment reduced stray light by as much as $10^{-8}$ at a wavelength of 2 nm from the probing laser, where the LTS signal is observed. The measurement period per pulse is 15 ns (5 ns ×3 bin), which is short enough to reduce the influence of light emitted from the plasma.

The estimated Thomson scattered photon number is so small that we used a photon counting method. The detected Thomson scattering signals were analyzed by a photon counting mode after more than 10,000 laser shots had been accumulated. The data accumulation process technique, taking advantage of the DC or repetitive operation of some discharges, was first suggested as a means of lowering the limiting electron densities by Sakoda *et al.*[11] The scattered signal, the background plasma emission and the stray light are small enough not to consider the multiple photons striking the photocathode. The photons were counted for three configurations at each test condition: 1) with plasma and laser, 2) with plasma
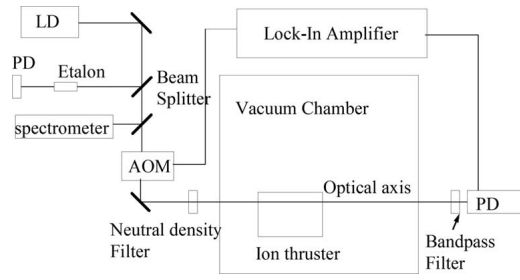
FIG. 3. Experimental setup for LAS measurements.

and without laser, and 3) with laser and without plasma. We evaluated the actual LTS signal by subtracting the number of photons obtained for configurations 2 and 3 from the number of photons obtained for configuration 1. Given the presence of the TGS and the short measurement period, the stray light and emission light from the plasma is fairly low. Therefore, the SNR (signal to noise ratio) is above five at all conditions and the largest noise is the shot noise, which can be estimated as the square root of total photo-electrons due to Thomson scattering, plasma emission and stray light.[10] The application of laser Thomson scattering technique to the measurement of plasma property in the ion thruster has been validated in our previous study.[12,21]

## C. Laser absorption spectroscopy

Figure 3 shows a diagram of the experimental setup for LAS. We use a laser diode to measure the transition line of xenon at 823.16 nm ($5p^5(^2P^\circ_{3/2})6s\ ^2[^3/_2]^\circ$ - $5p^5(^2P^\circ_{3/2})6p\ ^2[^3/_2]$). The transition data for this measurement are shown in Table II (from the NIST database[22] and Ref. 15). The mode-hop free tuning range of the laser is about 30 GHz. The laser output power is ~30 mW with a power of ~0.1 mW injected into the ion thruster through the neutral density filter in order to prevent saturation.[23] The diode laser is set for a 25 GHz mode-hop-free sawtooth frequency scan every 5 seconds (up and down scan in 10 s). An optical isolator is used to prevent back reflection into the laser. Light is detected by a photo diode (PD) outside the vacuum chamber. A dielectric interference filter (10 nm band-pass, center wavelength of 820 nm) and an iris are used to suppress background light and emission from the plasma.

To improve the signal-to-noise ratio (SNR), we use an acousto-optic modulator (AOM) and a lock-in amplifier. The laser is chopped at 1 kHz by the AOM and the modulated signal is detected by the lock-in amplifier. A solid etalon (free spectral range = 1.15 GHz) is used as a frequency reference and a spectrometer is used for coarse frequency measurement.

TABLE II. Transition data for target xenon line from NIST database (Ref. 21).

| $\lambda$, nm (Air) | $E_i$, eV | $E_k$, eV | $A_{ki}$, s$^{-1}$ | $g_i$ | $g_k$ |
|---|---|---|---|---|---|
| 823.16 | 8.315 | 9.821 | $2.5 \times 10^7$ | 5 | 5 |

All signals are recorded using a PC-based data acquisition system and a 100 KHz 16-bit A/D module.

## III. RESULTS AND DISCUSSION

### A. Effect of laser intensity on Thomson scattering signal

The thresholds of the laser intensity on these conditions were investigated, since the laser induced some perturbation in the xenon plasma due to photo-ionization of the excited xenon atoms. We focus here on the metastable xenon atoms. There are four metastable states that can be ionized by the incident laser; the energy levels are 8.315 eV, 8.437 eV, 9.447 eV, 9.570 eV, respectively. If the wavelength of the laser is 532 nm (photon energy is 2.3 eV), metastable atoms absorb three photons; two photons for multi-photo-ionization (ionization energy is 12.13 eV) and one photon for Thomson scattering. Thus, the signal count in photo-ionization from metastable atoms is proportional to the cube of the incident probe laser energy, $E_L$. On the other hand, the Thomson scattering signal is proportional to $E_L$.

Figure 4(a) shows the relation between the signal count at a wavelength of 530.5 nm and the incident laser energy at a xenon mass flow rate of 20 $\mu$g/s and incident microwave power of 6 W using an *f*-theta lens. The signal count is proportional to $E_L$, at $E_L < 50$ mJ and then it is proportional to $E_L^3$. Therefore, when $E_L < 50$ mJ, photo-ionization effect can be negligible. 50 mJ is not, however, enough energy to measure plasma properties in this plasma. Photo-ionization is nonlinear, so the possibility of photo-ionization will be
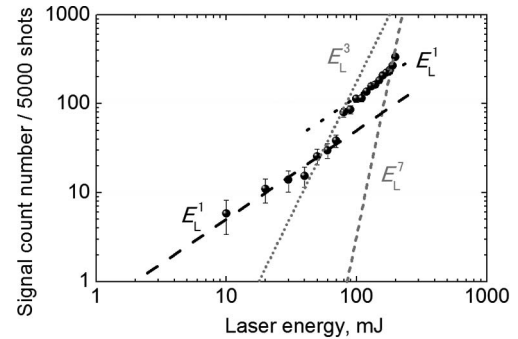


(a)
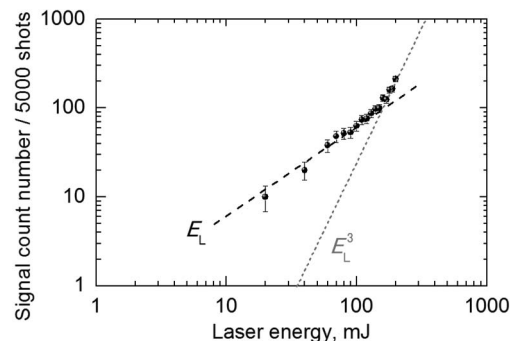


(b)

FIG. 4. Signal count number vs. laser energy. a) using $f = 200$ mm f-theta lens b) using using $f = 200$ mm plano-convex lens. $P_i = 6$ W, $\dot{m} = 20$ $\mu$g/s.

decreased if the laser intensity is decreased at the observed volume. Therefore, a plano-convex lens was used instead of the f-theta lens. The spot size of the plano-convex lens is about 165 $\mu$m, it is two times larger than that of the *f*-theta lens. Figure 4(b) shows the relation between the signal count and $E_L$ using the plano-convex lens. The threshold laser energy, $E_{critical}$, increases to 150 mJ; at $E_L < 150$ mJ, the signal count number is proportional to $E_L$ and then it is proportional to $E_L^3$. The threshold intensity using the plano-convex lens is $1.2 \times 10^{15}$ W/m$^2$, which is in good agreement with that using the *f*-theta lens, considering the 10 mm uncertainty of the spot size

In the case of the $f = 200$ mm *f*-theta lens, signal count number increases with $E_L^1$ at 90 mJ $< E_L <$ 180 mJ. This would be due to saturation; almost all the metastable xenon atoms are ionized by the probe laser. Therefore, the signal is proportional to $E_L^1$. At $E_L > 180$ mJ, the signal count number is proportional to $E_L^7$, this would be due to photo-ionization from the ground state xenon atoms. Since the ionization energy of xenon is 12.13 eV and the photon energy of 532 nm light is 2.3 eV, the ground state atoms absorb seven photons; six photons are needed for photo-ionization and one photon for scattering. Therefore, the signal shows 7$^{th}$ power dependence.

We investigate the thresholds for five mass flow rates; 5 $\mu$g/s, 10 $\mu$g/s, 20 $\mu$g/s, 30 $\mu$g/s and 40 $\mu$g/s. The thresholds of photo-ionization are almost the same when the mass flow rate is changed; the threshold for $\dot{m} = 5$ $\mu$g/s, 10 $\mu$g/s, 20 $\mu$g/s, 30 $\mu$g/s and 40 $\mu$g/s are 180 mJ, 140 mJ, 150 mJ, 170 mJ and 140 mJ, respectively, at incident microwave power of 6 W and using an $f = 200$ mm plano-convex lens.

## B. Number density and electron temperature measurement by LTS

The thresholds of photo-ionization using the $f = 200$ mm plano-convex lens are 140 mJ to 180 mJ, so the incident probe laser energy is set as 80 mJ. Figure 5 shows the measured Thomson scattering spectrum at $P_i = 6$ W and $\dot{m} = 20$ $\mu$g/s. From the shape of the Thomson spectrum, we conclude that the electron energy distribution function (EEDF) is Maxwellian, as in krypton propellant.[11] Thomson
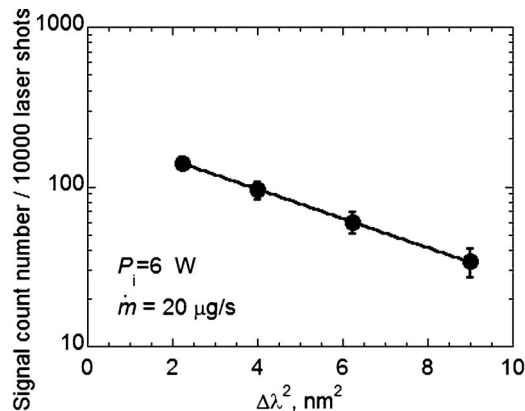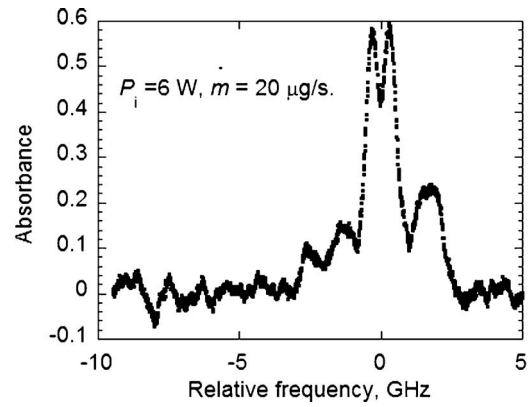


FIG. 6. Absorption profile of metastable xenon atom. $P_i = 6$ W, $\dot{m} = 20$ $\mu$g/s.

scattering spectra for various mass flow rates were measured, and all of the spectra can be fit by Gaussian. These results show that a flux tube model can be used to simulate the ion beam trajectory for the ion engine grid erosion evaluation code, and the calculation cost is much lower than that of the Full Particle in Cell (PIC) model.[24] Miyasaka *et al.*[25] show that there is no difference between the numerical results using the full-Particle In Cell (PIC) model and those using the flux tube model,[26,27] if the EEDF in the vicinity of the screen grid is Maxwellian. From this spectrum and the Rayleigh scattering calibration using nitrogen gas, $N_e$ and $T_e$ were calculated to be $(6.2 \pm 0.4) \times 10^{17}$ m$^{-3}$ and $2.2 \pm 0.4$ eV, respectively. The experimental uncertainty for each point was determined primarily by the statistical fluctuation in the number of detected photons.[28]

## C. Number density of metastable xenon atoms by LAS

Figure 6 shows the measured absorption spectrum of metastable xenon atoms at $P_i = 6$ W, $\dot{m} = 20$ $\mu$g/s. The spectrum was numerically integrated to estimate the metastable xenon atom population, though we can see hyperfine structure (isotope shift, nuclear spin splitting and anomalous Zeeman shifts). An electron excitation temperature is assumed to be the Measured Electron Temperature, as deduced from LTS, and the linear density of 6s [3/2]$^0_2$ metastable atoms is estimated to be $(3.4 \pm 1.7) \times 10^{15}$ m$^{-2}$. The large uncertainty comes from the uncertainty of the Einstein coefficient and the electron excitation temperature. If we assume that the absorber is uniformly present over a length, $l_{abs}$, and $l_{abs}$ is assumed to be 0.021 m, which is the inner diameter of the discharge chamber, the population of 6s [3/2]$^0_2$ metastable



FIG. 5. Spectrum of Thomson scattering. $P_i = 6$ W, $\dot{m} = 20$ $\mu$g/s, using f = 200 mm plano-convex lens, incident probe laser energy of 80 mJ.

TABLE III. Energy level and statistical weight of xenon metastable atoms from NIST database (Ref. 21).

| Configurations | $E_i$, eV | $g_i$ |
|---|---|---|
| 6s[3/2]$^0_2$ | 8.315 | 5 |
| 6s[3/2]$^0_2$ | 8.437 | 3 |
| 6s[1/2]$^0_2$ | 9.447 | 1 |
| 6s[1/2]$^0_2$ | 9.570 | 3 |

TABLE IV. Thresholds of photo-ionization at several test conditions.

| $\dot{m}$, μg/s | $P$, W | $E_{critical}$, mJ | $N_e$, m$^{-3}$ | $T_e$, eV | $N_m$, m$^{-3}$ | $N_e/N_m$ |
|---|---|---|---|---|---|---|
| 10 | 6 | 140 | $5.2 \times 10^{17}$ | 2.1 | $1.3 \times 10^{17}$ | 4 |
| 20 | 6 | 150 | $6.2 \times 10^{17}$ | 2.2 | $1.7 \times 10^{17}$ | 3.6 |
| 30 | 6 | 170 | $5.9 \times 10^{17}$ | 1.5 | $1.5 \times 10^{17}$ | 3.8 |
| 40 | 6 | 140 | $8.6 \times 10^{17}$ | 1.6 | $1.8 \times 10^{17}$ | 4.8 |

atoms, $N_m$, is estimated to be $(1.7 \pm 0.8) \times 10^{17}$ m$^{-3}$ (in this calculation of uncertainty, spatial distribution is not taken into account).

The sum of the number density of four metastable xenon atoms was estimated. In this estimation, the population in each metastable state, 8.315 eV, 8.437 eV, 9.447 eV, 9.570 eV, is assumed to be proportional to the statistical weight. Though this is only a rough estimate, it is sufficient for order of magnitude estimation. So the population of 8.437 eV, 9.447 eV, 9.570 eV is estimated as $1.0 \times 10^{17}$ m$^{-3}$, $3.4 \times 10^{16}$ m$^{-3}$, $1.0 \times 10^{17}$ m$^{-3}$, respectively, using the population of 8.315 eV of $1.7 \times 10^{17}$ m$^{-3}$ by LAS and the $g_i$ shown in Table III deduced from the NIST database.[21] Therefore, the sum of the four metastable populations is estimated to be $4.0 \times 10^{17}$ m$^{-3}$.

This value does not contradict the rough estimate of $6.2 \times 10^{17}$ m$^{-3}$ according to the Fig. 4(a), considering large uncertainty of the Einstein coefficient, the electron temperature and the rough assumptions, such as uniform plasma. That is, the second $E_L^1$ line (90 mJ $< E_L <$ 180 mJ) is due to the saturation of photo-ionized metastable atoms; all of the metastable atoms are ionized, so the signal is proportional to $E_L^1$. The number of detected photo-electrons in this regime is almost twice as large as the extension line of the non-saturation regime at $E_L <$ 90 mJ. This result shows that the total number density of metastable atoms is as high as the electron number density. Therefore, the estimated number density of total metastable xenon atoms, which can be two-photon ionized, is estimated to be almost the same as that of electrons, $6.2 \times 10^{17}$ m$^{-3}$.

Table IV shows the threshold of the photo-ionization from the metastable atoms and plasma properties for four mass flow rates. The electron number density increases with an increase in mass flow rate due to the increase in the pressure inside the discharge chamber.[11] Considering the uncertainty of the electron temperature, the electron temperature decreases with an increase in mass flow rate; this is because specific power (incident microwave power divided by mass flow rate) decreases with mass flow rate at constant incident microwave power. As mentioned above, the threshold is kept almost constant; the ratio of $N_e/N_m$ seems almost the same, considering the uncertainty of the populations, plasma density and electron temperature.

## IV. CONCLUSIONS

Xenon plasma properties were measured using the laser Thomson scattering technique (LTS) in a miniature ion thruster. The threshold of the probe laser intensity against photo-ionization in a miniature xenon ion thruster is $1 \times 10^{15}$ W/m$^2$. This value is almost constant for various mass flow rates, since the ratio of population of the metastable atoms to the electron number density is little changed. More detailed investigations will be needed to estimate the threshold intensity in various xenon plasmas; the populations of other metastable states, in particular, should be considered, and spatial distribution of metastable atom number density should be studied to evaluate the populations at the measurement point without assumption of the absorber length. On the other hand, even in the absence of more detailed investigation, we have demonstrated the applicability of the LTS technique to the measurement of xenon plasma for probe laser intensity below the threshold. The non-intrusive nature of the LTS could be applied to electric propulsion systems as well as ion thrusters; measurements near the magnetic poles or antenna in an RF thruster, or near the hollow cathode in a DC thruster, would reveal the plasma oscillation mechanism inside the discharge chamber. It could also help to illuminate the physics inside the acceleration channel and the plume in Hall thrusters.

[1] P. J. Wilbur, V. K. Rawlin, and J. R. Beattie, J. Propul. Power **14**, 708 (1998).

[2] J. S. Sovey, V. K. Rawlin, and M. J. Patterson, J. Propul. Power **17**, 517 (2001).

[3] A. Fujiwara, J. Kawaguchi, D. K. Yeomans, M. Abe, T. Mukai, T. Okada, J. Saito, H. Yano, M. Yoshikawa, D. J. Scheeres, O. Barnouin-Jha, A. F. Cheng, H. Demura, R. W. Gaskell, N. Hirata, H. Ikeda, T. Kominato, H. Miyamoto, A. M. Nakamura, R. Nakamura, S. Sasaki, and K. Uesugi, Science **312**, 1330 (2006).

[4] H. Kuninaka, K. Nishiyama, I. Funaki, T. Yamada, Y. Shimizu, and J. Kawaguchi, J. Propul. Power **23**, 544 (2007).

[5] S. Kitamura, H. Nagano, Y. Nakamura, I. Kudo, and K. Machida, J. Propul. Power **2**, 513 (1986).

[6] M. Nakano, Fron. Appl. Plasma Technol. **2**, 21 (2009).

[7] D. A. Herman and A. D. Gallimore, Rev. Sci. Instrum. **79**, 013302 (2008).

[8] J. Sheffield, *Plasma Scattering of Electromagnetic Radiation* (Academic, New York, 1975), Chap. 9.

[9] D. E. Evans and J. Katzenstein, Rep. Prog. Phys. **32**, 207 (1969).

[10] K. Muraoka, K. Uchino, and M. D. Bowden, Plasma Phys. Control. Fusion **40**, 1221 (1998).

[11] T. Sakoda, S. Momii, K. Uchino, K. Muraoka, M. Bowden, M. Maeda, Y. Manabe, M. Kitagawa, and T. Kimura, Jpn. J. Appl. Phys. **30**, L1425 (1991).

[12] N. Yamamoto, K. Tomita, N. Yamasaki, T. Tsuru, T. Ezaki, Y. Kotani, K. Uchino, and H. Nakashima, Plasma Sources Sci. Technol. **19**, 045009 (2010).

[13] Y. K. Kim, K. Tomita, S. Hassaballa, K. Uchino, K. Muraoka, H. Hatanaka, Y. M. Kim, S. E. Lee, S. H. Son, and S. H. Jang, SID Int. Symp. Digest Tech. Papers **35**, 550 (2004).

[14] A. L. Walsh, Spectrochim. Acta **7**, 108 (1955).

[15] M. Matsui, K. Komurasaki, G. Herdrich, and M. Auweter-Kurtz, AIAA J. **43**, 2060 (2005).

[16] M. Matsui, S. Yokota, H. Takayanagi, H. Koizumi, K. Komurasaki, and Y. Arakawa, AIAA Paper 2006–0767 (2006).

[17] N. Yamamoto, S. Kondo, T. Chikaoka, H. Masui, and H. Nakashima, J. Appl. Phys. **102**, 123304 (2007).

[18] N. Yamamoto, H. Masui, H. Kataharada, H. Nakashima, and Y. Takao, J. Propul. Power **22**, 925 (2006).

[19] R. E. Wirz, "Discharge Plasma Processes of Ring-Cusp Ion Thrusters," Ph. D. Dissertation, California Institute of Technology, April 2005.

[20] Y. Arakawa and K. Ishihara, *Proceedings of 22nd International Electric Propulsion Conference*, IEPC-91-118 (1991).

[21] K. Tomita, N. Yamamoto, N. Yamasaki, T. Tsuru, K. Uchino, and H. Nakashima, J. Propul. Power **26**, 381 (2010).

[22] NIST Atomic Spectra Database Lines Form, http://physics.nist.gov/PhysRefData/ASD/lines_form.html.

[23] M. Matsui, S. Ogawa, K. Komurasaki, and Y. Arakawa, J. Appl. Phys. **100**, 063102 (2006).

[24] V. Vahedi and M. Surendra, Comput. Phys. Commun. **87**, 179 (1995).

[25] T. Miyasaka, T. Kobayashi and K. Asato, Trans. Jpn. Soc. Artificial Intell., Aerospace Technol. Jpn. **8**, Pb_61 (2011).

[26] Y. Nakayama and P. J. Wilbur, J. Propul. Power **19**, 607 (2003).

[27] M. Nakano, T. Tachibana, and Y. Arakawa, Trans. Jpn. Soc. Aero. Space Sci. **45**, 154 (2002).

[28] H. J. Kunze, "The Laser as a Tool for Plasma Diagnostics," in *Plasma Diagnostics*, edited by W. Lochte-Holtgreven (North-Holland Publishing Company, Amsterdam, 1968), p. 550.